IEEE Robotics and Automation Letters (RA-L) paper, presented at ICRA 2026, Vienna, Austria. Cite as RA-L paper.

Plantar Compensation via Dynamic Control of Pneumatic Insoles for Flatfoot Deformity*

1st Bin Zhang
College of Mechanical and Electrical Engineering
China Jiliang University
Hangzhou, China
zjuzhangbin@zju.edu.cn

2nd Yan Guo
School of Mechanical Engineering
Zhejiang University
Hangzhou, China.
1429194044@qq.com

3rd Yijun Zhang
School of Mechanical Engineering
Zhejiang University
Hangzhou, China.
3284478644@qq.com

4th Yi Jingang
Department of Mechanical and Aerospace Engineering
Rutgers University
Piscataway, USA
jgyi@rutgers.edu

5th Binrui Wang
College of Mechanical and Electrical Engineering
China Jiliang University
Hangzhou, China
wangbrpaper@163.com

6th Tao Liu
School of Mechanical Engineering
Zhejiang University
Hangzhou, China.
liutao@zju.edu.cn

7th Wenyang Li
Zhiyuan Research Institute
Hangzhou, China
lwy341449996@hotmail.com

8th Long He
Zhiyuan Research Institute
Hangzhou, China
helong@zy-cs.com.cn

***Abstract*—Human feet are crucial for supporting body weight and adapting to complex terrains. Adult-acquired flatfoot deformity (AAFD) arises from congenital or acquired causes, impairing the foot's ability to transition between flexible and rigid states, known as the lock-unlock mechanism during the stance and swing phases. In this study, we propose a plantar dynamic support system that utilizes pneumatic airbags, regulated through a model predictive control (MPC) strategy to minimize tracking errors. Experiments were conducted to measure kinetic parameters and electromyography signals, validating the system's efficacy. The results showed improvements in the normalized navicular height truncated (NNHt) index and reductions in muscle activity of the fibularis longus (FL), soleus (SOL), and gastrocnemius (GAST) by 4.42%, 16.65%, and 23.84%, respectively, during the stance phase.**

***Index Terms*—Wearable Robotics, Plantar Dynamic Support, Pneumatic Insoles**

I. Introduction

HUMAN foot is a complex anatomical structure consisting of 26 bones, 33 joints, 20 muscles, 114 ligaments, and an extensive network of nerves and vessels [1]. It is vital for weight-bearing and movement, including walking, running, and jumping. Structural stability is maintained by the medial and lateral longitudinal arches (MLA and LLA, Fig. 1), which facilitate shock absorption [2], optimize plantar pressure distribution [3], and enhance adaptability [4]. Flatfoot deformity, encompassing congenital (CFD) and AAFD forms, results from congenital or acquired factors, with posterior tibial tendon dysfunction (PTTD) being a primary cause [5].

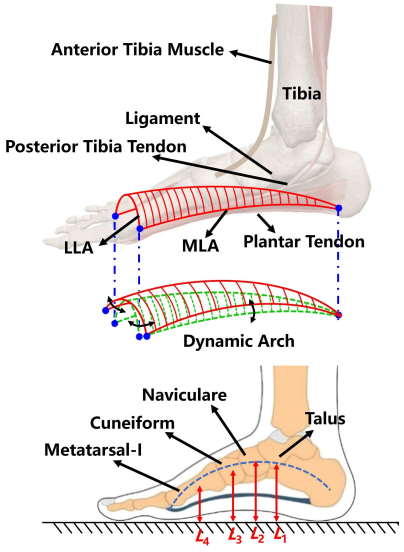

Fig. 1. The shape and the dynamic motion of arch.

During the gait cycle, feet transition from a flexible state in the swing phase to a rigid state in the stance phase. Flexibility aids adaptability to uneven terrain, while rigidity enables the foot to act as a lever, facilitating propulsion via the gastrocnemius-soleus complex [6]. In PTTD patients, the

This work was supported in part by Zhiyuan Laboratory under Grant No. ZYL2024006, and NSFC Grant No. 52175033. It was supported by the Clinical Research Ethics Committee of First Affiliated Hospital, College of Medicine, Zhejiang University under identification code No. 2020-80.

inability to lock the MLA and LLA results in a "bag of bones" deformity. Researchers [7] emphasize preventing flexible deformities from becoming rigid, as asymptomatic flatfoot can progress to symptomatic conditions due to degenerative processes.

The severity of foot arch collapse is clinically categorized into four grades (I-IV): mild, moderate, severe, and very severe [8]. AAFD grading is determined through patient history, physical examination, and medical imaging. Physical assessment involves visual inspection of arch flattening, tenderness palpation, and foot function evaluation. Orthotic devices are commonly recommended for PTTD conservative management. Neville et al. [9] demonstrated that the AirLift PTTD brace effectively reshapes the foot through hindfoot inversion, forefoot dorsiflexion, and adduction. Semciw et al. [10] found that custom foot orthotics reduced gluteus medius activity by 43%, though fixed-shape orthotics may not benefit all muscles, necessitating consideration of lock-unlock mechanisms [6]. Ozmanevra et al. [11] investigated the effects of various insole materials on kinetic and kinematic parameters, while Zhang et al. [12] developed tunable airbags that optimally reshape foot arches with 15% body weight force.

Current arch braces, typically constructed from silica gel or polyurethane, exhibit stable and elastic mechanical properties. Studies show that fixed-shape braces redistribute plantar pressure by reducing hindfoot load and increasing midfoot peak pressure [4]. However, customizing insoles for patients with varying foot sizes and PTTD severity remains challenging, requiring individualized 3D foot modeling [13]. Orthotics must also be periodically replaced due to foot degeneration or device dysfunction. Prolonged use of passive orthotics risks disuse atrophy, user dependency [14], and neural adaptations from reduced muscle activity [15]. Thus, passive orthotics are best suited for short-term use, while long-term solutions should aim to restore intrinsic muscle function by replicating normal arch biomechanics.

Foot orthotics effectively alleviate pain and fatigue by arch reshaping. PTTD triggers compensatory knee valgus and hip extorsion, increasing inflammation risks in lower extremities [16]. Wearable exoskeletons offer force assistance alternatives [17], [18]: Park et al. [19] employed four pneumatic muscles (PMs) for ankle rehabilitation, enabling plantar/dorsiflexion and varus-valgus rotation, though efficacy remains unvalidated. Zhang et al. [20] designed a lightweight modular cable-driven ankle exoskeleton, while Sridar et al. [21] implemented gait-adaptive stiffness control via soft actuators. Wang et al. [22] developed paraplegia balance-support exoskeletons. Notably, Boes et al. [23] reported a portable ankle-foot orthosis failed to improve endurance in six-minute walking tests.

The PM-driven exoskeletons offer assistance for compensating muscle force deficits. Studies have shown that kinematic behavior can be modulated by adjusting pneumatic muscles in response to motion intent [19], and that even passive exoskeletons can reduce metabolic cost [24]. However, prolonged use of such devices may lead to disuse atrophy in PTTD patients, as extrinsic muscles compensate for intrinsic dysfunction. Notably, these systems fail to adequately relieve plantar muscles or correct arch deformities, highlighting limitations in addressing the root causes of PTTD.

The primary aim of this study was to propose a plantar pneumatic arch supporting system as an alternative to traditional orthotic insoles with implementation of gait-synchronized control mechanism. The second aim was to investigate the immediate effect of foot orthoses on calf muscle activity (FL, SOL, GAST) during walking in healthy and AAFD patients.

II. Design of the Plantar Dynamic Support System of Pneumatic Insole

A. Plantar Biomechanic Modeling and Human Arch Measurement

To achieve dynamic plantar pressure support, a 3D finite element model (FEM) of a healthy foot was developed, as illustrated in Fig. 2. The modeling process, depicted in Fig. 2(a), comprises five stages: computed tomography (CT) scanning, surface reconstruction, material configuration, loading and solving, and analysis. Following prior research [25], 28 participants (14 healthy, 14 AAFD patients) were recruited, with 10 diagnosed as Grade II and 4 as Grade III flatfoot based on clinical and radiographic criteria. CT data from one healthy participant were used to construct the model, which included 19 bones, 7 ligaments, and 5 tendons, labeled as ② and ③ in Fig. 2(b). Tetrahedral meshing was performed using Ansys Workbench V15.0, with the meshed model shown as ④ in Fig. 2(b).

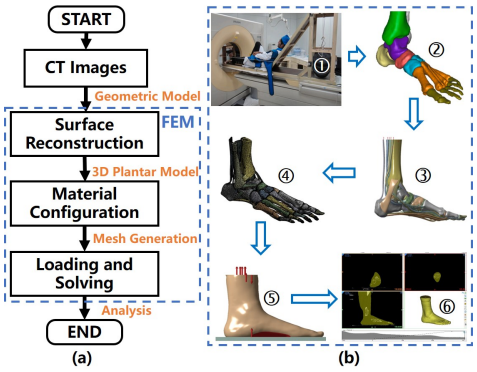

Fig. 2. (a) Modeling process based on finite element method. (b) Model illustration at different stages.

Consistent with prior research [25], all tissues were modeled as continuous, homogeneous, and isotropic linear elastic materials, except for cartilage and joints, which were treated as hyperelastic materials. Utilizing CT images from six volunteers, four key points on the medial longitudinal arch (MLA) were identified, corresponding to the talus, navicular, central cuneiform, and first metatarsal. The vertical distances from these points to the ground, denoted as L_1, L_2, L_3, and L_4, respectively, were measured, as illustrated in Fig. 3 (a).

Plantar force loading was analyzed via FEM. The reduction in perpendicular height under varying loading conditions was compared with that of a normal foot model, as shown in

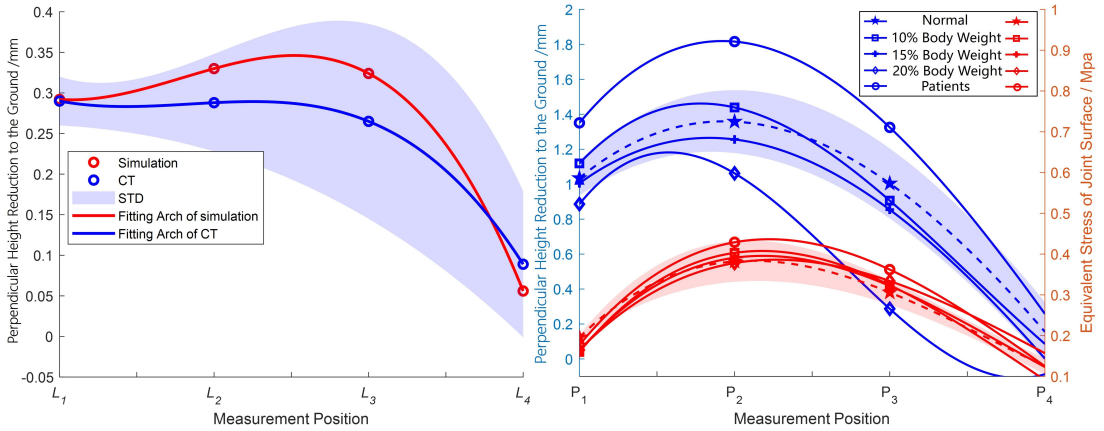

Fig. 3. (a) Arch measurement based on CT. (b) Model illustration at different stages.

Fig. 3 (b). Blue and red curves indicate normal vertical displacement and joint deformation ranges, respectively. The results indicate that 10% to 15% of body weight represents the optimal plantar pressure for maintaining arch integrity. Pressures exceeding or falling short of this range—caused by either excessive loading or weakened plantar fascia (PF)—lead to abnormal deformations. The equivalent pressure trends align with distance reduction, and the pressure remains within the normal range when external forces are applied to the foot.

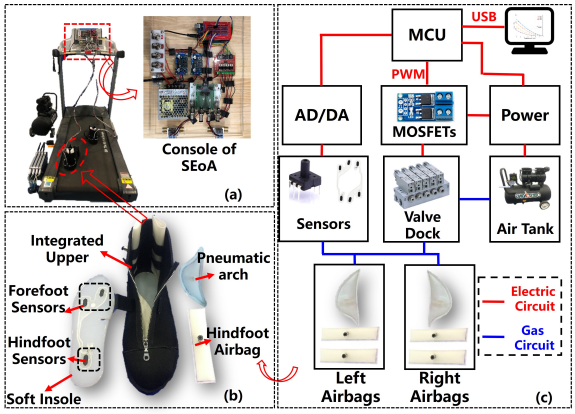

Fig. 4. The structure of the plantar dynamic support system of pneumatic insole. (a) The overall system applied in treadmill. (b) The fabricated shoe including soft insole, plantar airbag, hindfoot airbag, plantar pressure sensor and upper. (c) The console structure of the system.

B. System Construction

The airbags were fabricated with an inner thermoplastic polyurethane elastomer (TPU) layer and an outer nylon fabric. TPU film was laminated onto one side of the nylon substrate to create an adhesive interface, which was then thermally bonded to the TPU-coated nylon reinforcement sheet using a hot press with optimal lamination temperature at 170°C. To ensure both comfort and elasticity, the insoles were fabricated using gelatin material, with reserved spaces for integrating plantar airbags and pressure sensors. Nylon cloth was shaped and sealed with a zipper to form the shoe cover. TPU can withstand 40 kPa pressure and it can be improved to 400 kPa by the nylon fabric. The structure of the soft exoskeleton of arch (SEoA) is shown in Fig. 4.

An Arduino Mega 2560 (Arduino, Italy) was employed as the microcontroller. The air pressure of the airbags was detected by an air pressure sensor (XGZP6857, CFsensor, China) and the plantar pressure were detected by flexible pressure sensor. Four switching valves were used to control the inflation and deflation processes both of the hindfoot and plantar airbags. The valve dock (SMC V114-5GZ, SMC, Japan) enables high-frequency switching, with opening and closing times of less than 5 ms and 4 ms, respectively. The valves were driven by a switching board (MOSFET IRF540, SANYO, Japan) with pulse width modulation (PWM) waves.

C. Validation of Airbags' Performance

Static pressure was tested by a pressure tester (ZQ990B, ZHIQU, China) and the height of airbags, pressure value, and the inner air pressure are recorded. During the test, the plantar airbag was inflated from 40 kPa to 200 kPa and the height of the plantar airbag was changed from 15mm to 0. The displacement, air pressure, and force represent the height change, inner pressure change, and output force of the plantar airbag, respectively. With fixed air pressure, the relationship between force and the displacement can be fitted by a quadratic function with air pressure fixed. The stiffness of the airbag is linearly increasing with growing displacement. The output force could be fitted as Eq. (2).

The airbags were designed to replicate the shape of the MLA. It is hard to establish the accurate model of the airbags. Under open-loop control, the relationship between internal pressure and PWM duty ratio was modeled using a sigmoid function for inflation and an exponential function for deflation.

$$\begin{cases} f_{inflation} = \dfrac{a_1}{1 + e^{a_2(x-a_3)}} \\ f_{deflation} = b_1 + b_2 e^{b_3(x-\tau)} \end{cases} \tag{2}$$

where $f_{inflation}$ and $f_{deflation}$ represent the pressure during inflation and deflation process, respectively. τ is the delay time of deflation. a_i and $b_i, i = 1, 2, 3)$ are fitted as:

$$\begin{cases} a_i = \dfrac{a_{i1}}{1 + e^{a_{i2}(x - a_{i3}) + a_{i4}}} \\ b_i = b_{i1} + b_{i2} e^{b_{i3}(x)} \end{cases} \tag{3}$$

where a_{ij} and b_{il} are constant parameters representing the j_{th} and l_{th} coefficient of a_i and b_i.

$$\begin{cases} F_{airbag} = k_1 H^2 + k_2 H + k_3 \\ k_1 = a_1 P + a_2 \\ k_2 = b_1 P + b_2 \\ k_3 = c_1 P + c_2 \\ h \in (0, 15mm), P \in (0, 200kPa) \end{cases} \tag{4}$$

where F_{airbag} is the output force of the airbag. H is the height of the airbag, and P is the inner pressure. $a_1 = 2.6 \times 10^{-4}$, $a_2 = 8.7 \times 10^{-2}$, $b_1 = 1.95 \times 10^{-3}$, $b_2 = -1.32 \times 10^{-2}$, $c_1 = 1.2 \times 10^{-3}$, and $c_2 = 3.9 \times 10^{-1}$.

The output force characteristics of the airbag during a complete inflation-deflation cycle. A pronounced hysteresis effect is observed between the inflation and deflation phases, primarily attributable to the viscoelastic properties of the TPU material. This material dependency causes a temporal lag in the deflation response relative to the inflation process. The hysteresis behavior can be quantitatively described using Equation (2).

D. Model Predictive Control (MPC) Based Air Pressure Tracking

The model of pneumatic insole was fitted based on experiment. We introduce proportional-integral-differentiation control and MPC into air pressure tracking. The MPC diagram is illustrated in Fig. 5.

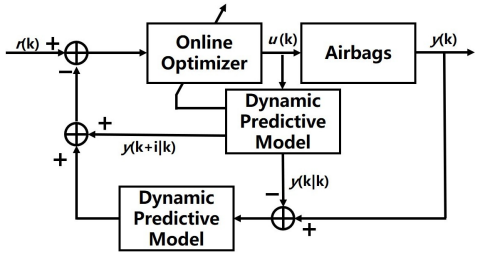

Fig. 5. Model Predictive Control (MPC) diagram of the plantar dynamic support system.

The model of plantar dynamic support system is described by:

$$y(k) = f(u(k), k) \tag{5}$$

where, $u(k) \in R^n$, $u(k) \in R^l$. And f represents the system. The $y(k)$ is the output and $u(k)$ is the control law which is duty ratio of PWM wave. The k represents the moment in iteration ($k = 0, 1, 2, ..., N$).

The input is defined as:

$$r(k+1), r(k+2), r(k+3), \cdots, r(k+p) \tag{6}$$

where $r(k+p)$ represents $(k+p)^{th}$ reference target which is a sinusoidal function in the system. The predictive output in several future period could be described as:

$$y_p(k+1|k), y_p(k+2|k), y_p(k+3|k), \cdots, y_p(k+p|k) \tag{7}$$

where p is the predictive moment in time domain which is defined to be 6. The $y(k+p|k)$ represents the predictive output at $(k+p)^{th}$ time based on the output at k^{th} time. The predictive control input is defined as:

$$Uk = u(k|k), u(k+1|k), u(k+2|k), \cdots, u(k+p-1|k) \tag{8}$$

The output and control law are constrained a certain range.

$$\begin{cases} y_{min} \leqslant y(k) \leqslant y_{max} \\ u_{min} \leqslant u(k) \leqslant u_{max} \end{cases} \tag{9}$$

where $y(k) \in$[0,200] ans $u(k) \in$[0,1].

The MPC minimizes the objective function:

$$J(y(k), Uk) = \sum_{i=k+1}^{k+p} (r(i) - y_p(i|k))^2 \tag{10}$$

In fact, the MPC is reduced to an optimization problem. The optimization process terminates once the objective function meets a predefined tolerance. The optimization target is defined as:

$$J(y(k), Uk) < \epsilon \tag{11}$$

where, ϵ is the tolerable accuracy. In this system, ϵ is set to be 0.03. In addition to the MPC approach, we compare its performance against that of a proportional–integral–derivative (PID) controller.

The track error in PID control can be calculated as Eq. (12), where $y_d(k)$ is the tracking target and $y^{'}(k)$ is the output of the system.

$$e(k) = y_d(k) - y^{'}(k) \tag{12}$$

The control law is defined as

$$u(k) = \Gamma e(k) + \Psi \sum_{i=0}^{k} e(i) + L \frac{e(k) - e(k-1)}{T_s} \tag{13}$$

where, L, Γ, and Ψ are control gains. During control, the $e(k)$ and $u(k)$ are recorded and L =0, and Γ =0.45, and Ψ =0.72.

III. SYSTEM VALIDATION AND EXPERIMENT

A. Sensor-based Gait Detection

The airbags' inflation and deflation must adapt to gait events to provide dynamic support. During the gait cycle, feet transition from a flexible state in the swing phase to a rigid state in the stance phase [6]. The cycle was divided into arch-locked and arch-unlocked stages, with airbag timing synchronized accordingly.

Plantar airbags simulate the MLA, improving pressure distribution during stance. Hindfoot airbags inflate during early stance and late swing, and deflate during late stance and early swing. Plantar airbags support the MLA and prevent hindfoot valgus, whereas hindfoot airbags stabilize the ankle joint, improve balance, and correct valgus. Gait detection, achieved via soft pressure sensors (two forefoot, one hindfoot) at 50Hz, utilized experimentally determined contact and leave thresholds for forefoot and hindfoot.

B. Performance of System Control

The step response and tracking experiment are conducted to tested the time and frequency response performance of the controller. Nine step response experiments were conducted by setting the target pressure from 40 kPa to 200 kPa. As shown in Fig. 6 (a), the maximum and minimum rising times are 0.48s and 0.1s, respectively. The system reached 200 kPa in 0.48s and the rising time was reduced when the target pressure decreased.

Sinusoidal tracking experiments were conducted across varying frequencies, employing eight distinct input periods ranging from 0.25s to 4s (Fig. 6 (c)). Both controllers effectively tracked input signals at frequencies below 1 Hz; however, phase lag between the target and output increased with frequency. As illustrated in Fig. 6 (b), the operational bandwidths of both PID and MPC controllers spanned 0 to 1.5Hz. The initial MPC parameters were systematically determined through empirical optimization based on conventional PID control methodology.

C. Plantar Pressure Compensation Experiment

Walking experiments were conducted with ten volunteers—four with AAFD and six healthy controls. The mean age, height, and foot length of the healthy subjects were 26.3±2.2 years, 174.8±10.0 cm, and 267.5 ±8.8 mm, respectively. The AAFD group had a mean age of 39.0 ± 11.5 years, height of 170.0 ± 1.8 cm, and foot length of 260.0 ± 2.2 mm. This study was reviewed and approved by the Ethics Committee of the First Affiliated Hospital, College of Medicine, Zhejiang University. The volunteers signed an informed consent form for the experimental protocol and purpose. We introduced six-minute walking test (6MWT), which is used to access gait [28]. Kinematic parameters and EMG were recorded. The process of 6MWT contains 1-minute standing before walking, 6-minute walking, and 1-minute standing after walking on the treadmill with the speed of 4 km/h.

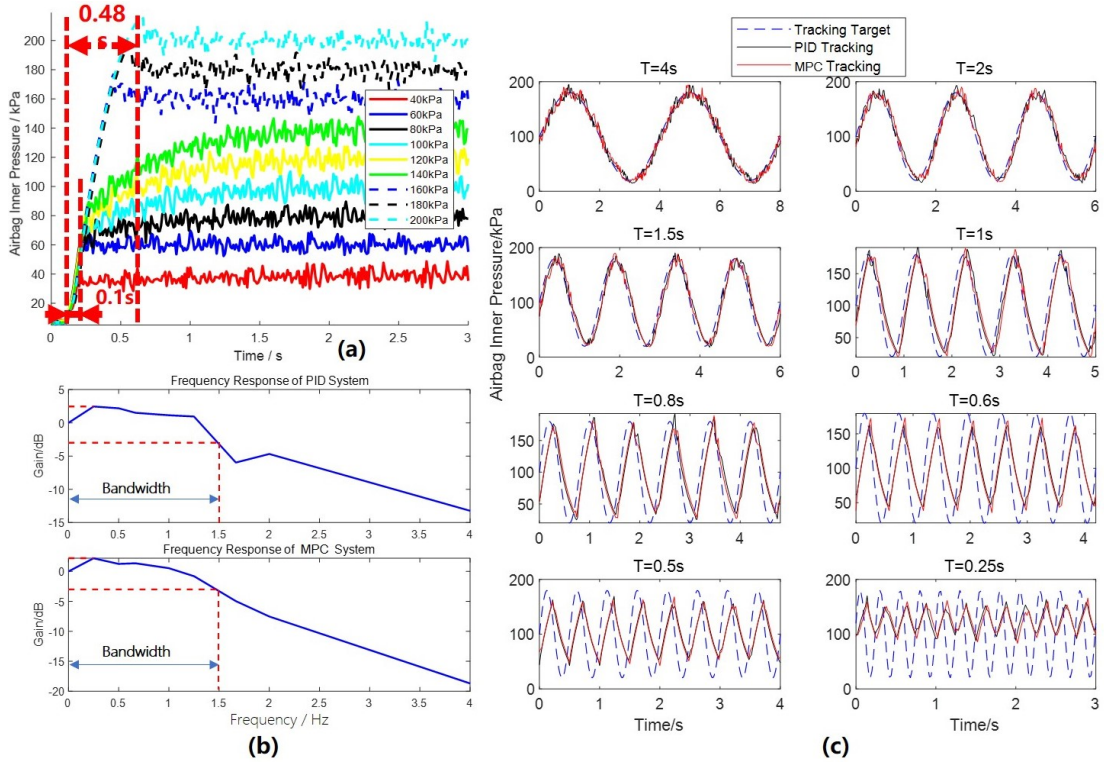

Fig. 6. The experiment of frequency response of the system. (a) Experiments of step responses in different air pressure of system. (b) The bandwidth of the PID and MPC. (c) The response of plantar dynamic support with different input frequency (period T).

To validate the arch-reshaping performance of plantar dynamic support system, kinematic parameters were recorded by VICON system with 100Hz sampling frequency during walking. The normalized navicular height truncated (NNHt) was calculated [29], which is the index of evaluating the effectiveness of AAFD rehabilitation clinically with shaded regions denoting standard deviation intervals, as illustrated in Fig. 7.

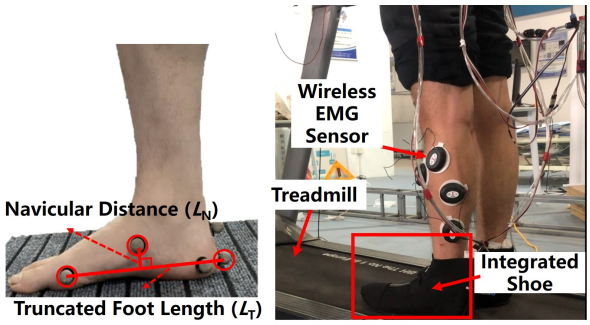

Fig. 7. Measurement methods of the NNHt. The NNHt index is calculated by:$NNHt = \frac{L_N}{L_T}$

The NNHt index of healthy volunteers significantly exceeds that of AAFD volunteers. While healthy volunteers show no notable NNHt differences with or without SEoA, substantial errors are evident in the red curves in Fig. 8. In contrast, AAFD volunteers exhibit significant NNHt variations depending on SEoA inclusion, suggesting greater utility in arch reshaping for AAFD individuals, whose feet struggle to adapt to inflated airbag shapes. Wearing pneumatic insoles improved the NNHt index, with AAFD volunteers showing a greater average increase (0.014) compared to healthy volunteers.

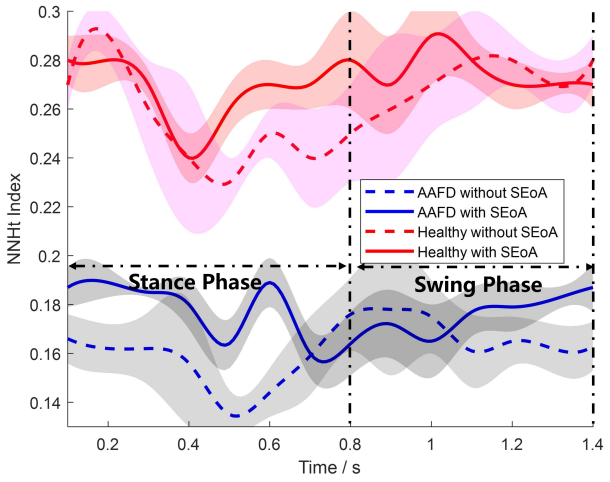

Fig. 8. The results of NNHt index of the volunteers.

The activities of the tibialis anterior (TA), fibularis longus (FL), soleus (SOL), and gastrocnemius (GAST) muscles were recorded. Baseline removal was achieved by subtracting the mean value from the raw signal, followed by Butterworth filtering. Subsequent processing included rectification, envelope calculation, and normalization. The normalized EMG signals (NES) across one gait cycle under three conditions are shown in Fig. 9.

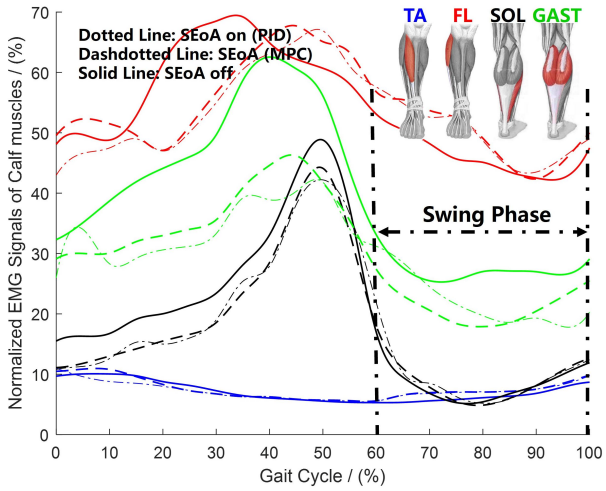

Fig. 9. EMG reduction performance of the calf muscles in walking experiment.

Solid, dotted, and dash-dotted lines denote the system in the off state, PID-controlled operation, and MPC-controlled operation, respectively. The blue, red, black, and green lines represent the EMG results of the TA, FL, SOL, and GAST, respectively. During stance phase, active system operation reduced NES in FL, SOL, and GAST compared to inactive states, while only GAST showed reduced NES during swing phase. TA exhibited minimal NES changes. Both PID and MPC controllers demonstrated similar NES reduction patterns, though identifying the superior control strategy for NES minimization remains unresolved.

To assess muscle fatigue, median frequency (MF) was computed from EMG signals. This involved preprocessing the signals within defined time windows, applying fast Fourier transform to obtain power spectral density, and subsequently calculating the average frequency across multiple windows. MF was determined as follows:

$$MF = \frac{1}{2}\int_{f_1}^{f_2} P(f)df \tag{14}$$

where, f_1 and f_2 are the upper and lower limits of EMG frequency respectively which are defined to be 20 Hertz, 450 Hertz generally [30]. $P(f)$ is the power spectral density. Power spectral density is the amount of power at each frequency of the EMG signal which is the mean power in 1 Hertz bandwidth. Since the data processing process is based on MATLAB and the $P(f)$ can be directly obtained. As shown in Table I, the MF reduction of muscle activity varies between healthy and AAFD patients. During stance, MF reduction in four muscles exceeds swing phase reductions, with AAFD patients showing larger decreases. No significant difference emerged between PID and MPC strategies. Posterior muscles

(SOL and GAST) demonstrated more reduction compared to anterior muscles (TA and FL). These reductions align with NES performance across the gait cycle (Fig. 9).

TABLE I
AVERAGE REDUCTION OF MF FOR BOTH HEALTHY AND AAFD VOLUNTEERS.

Average Reduction of MF (%)		**TA**	**FL**	**SOL**	**GAST**
Stance phase of AAFD Volunteer	PID	-1.20	4.42	16.65	23.84
Swing phase of AAFD Volunteer	PID	-15.31	-7.05	-4.13	-18.30
Stance phase of AAFD Volunteer	MPC	-1.32	3.24	17.87	22.21
Swing phase of AAFD Volunteer	MPC	-16.10	-5.86	-5.01	-16.88

IV. DISCUSSION

Individuals may develop AAFD due to congenital or acquired factors. The lock-unlock mechanism of the foot enables terrain adaptability and efficient forward propulsion during the gait cycle. Arch dysfunction can lead to serious complications, including compensatory joint mechanics, inflammatory conditions in the lower limbs, and chronic lower back pain. This study presents a novel contribution through the development of a soft exoskeleton system specifically designed for arch support and rehabilitation.

Plantar force loading experiments using the FEM method showed that a reduction in MLA vertical distance is acceptable when external pressure ranges from 10% to 15% of body weight. The external force correlates positively with body weight. No literature has addressed the optimal foot arch support. Venkadesan et al. [31] studied foot stiffness using fresh-frozen cadaveric feet, categorized into normal and abnormal with a transversal cut. Three-point bending tests revealed a quadratic relationship between loading force and displacement, with the arch providing up to 33% of body weight. In our study, the stiffness of the pneumatic arch resembled that of biological tissue, providing up to 23% of body weight support—an acceptable value considering that a full transverse cut completely eliminates arch support.

We conducted a comparison of the results by the proposed design and those relevant studies. Table II lists the comparison results. The comparison evaluation of orthopedic insole performance are assessed from three distinct aspects, that is, maximum navicular height truncated (NNHt), and max decrease in calf EMG. Note that existing research work shows different evaluation metrics and no study covers all of them, revealing a notable absence of unified evaluation criteria. Nevill et al. [9] measured hindfoot eversion degree to validate the AirLift PTTD brace. Greater hindfoot inversion was observed with air bladder inflation during the second rocker (mean: 1.7 degree; range, -0.7 to 6.1 degrees). We calculated NNHt to manifest the structural change; see [29]. For the proposed design, a significant improvement of 0.02 and 0.016 for NNHt was observed in patients and healthy volunteers, respectively.

TABLE II
QUANTITATIVE COMPARISONS WITH RELATED STUDIES.

References	**Max NNHt**	**Max EMG Decrease in Calf Muscle(%)**
Nevill et al. [9]	0.22	—
Semciw et al. [10]	—	30
Nawo. et al. [32]	—	37.5
Murley et al. [33]	—	19
Our Study	0.19	23.84

Prefabricated foot orthoses reduced gluteus medius and minimus activity by up to 43% during 2% to 13% of the gait cycle in healthy adults [10]. Smaller changes were observed for selected calf (medial gastrocnemius up to 30% reduction). The proposed system achieved similar performance in reducing muscle activity of SOL and GAST (medial gastrocnemius up to 23.84% reduction) with those results in [10]. And the timing of muscle activity reduction occurred at the similar moment. It implies that the pneumatic insoles resulted in reduction of muscle activity. However, the comprehensive effectiveness in one gait cycle is different. The dynamic compensation was positive to reduce muscle activity in stance phase but negative in swing phase. This might be caused by the soft bottom of the shoe that failed to provide continuous support in swing phase. Greater reductions in AAFD patients versus healthy subjects imply compensatory motion replacement.

From the current comparative results, our system exhibits superior performance in providing arch support for orthotic correction. Furthermore, it achieves comparable efficacy to orthopedic insoles in terms of reducing muscular activation levels. It remains unclear if improvement over days or weeks would be achieved and additional experiments need to be conducted on AAFD patients. For the healthy subjects, the NNHt was not improved in early stance phase and late swing phases. This might be caused by the soft bottom of the fabricated shoe that led force losing. In other phase (i.e., 10%-85% gait cycle), the supporting performance is validated.

Both the PID and MPC methods shared the similar performance in tracking sinusoid input in terms of tracking sinusoid input. However, the PID parameters were obtained based on artificial selection. And the MPC parameters were obtained based on constraints optimization which is more efficiency. MPC provides a promising way to realize better performance when it comes to improving adaptive speed regulation and adaptive control parameters in different process of treatment or rehabilitation. The deflation can not track the target well because the hystersis of deflation is mostly caused by the air flow resistance and the low elasticity of the inner layer in airbags. To decrease the flow resistance, short and wide air tube should be used.

The system presents three main limitations. First, its portability is constrained by the bulky compressor and flexible air

tank, necessitating future design modifications. Second, the study requires additional AAFD patient volunteers to validate plantar pressure compensation efficacy. Finally, control performance could be enhanced through optimized inflation-deflation processes and implementation of adaptive algorithms for speed regulation, parameter adjustment, and external load compensation [34].

V. CONCLUSIONS

A bio-inspired pneumatic insole featuring a dynamic structure that delivers periodic extrusion to the arch, aligning with the foot's lock-unlock mechanism during the gait cycle was proposed. This work establishes a foundational framework for exploring the impact of pneumatic insoles in individuals with symptomatic ankle and foot conditions. Future iterations may incorporate optimization based algorithms to enable adaptive speed regulation, adaptive control parameters, and adaptive performance with external loads.

REFERENCES

[1] G. C. Berlet, "PesPlanus(Flatfoot): Background, Anatomy, Pathophysiology," in *Medscape*, 18, Apr., 2021.

[2] R. C. Aland, and A. C. Sharp, "Anomalous plantar intrinsic foot muscle attaching to the medial longitudinal arch: possible mechanism for medial nerve entrapment: a case report," *J. Med. Case Rep.*, vol. 15, no. 1, Feb. 2021.

[3] R. Periyasamy, and S. Anand, "The effect of foot arch on plantar pressure distribution during standing," *J. Med. Eng. Technol.*, vol. 37, no. 5, pp. 342-347, 2013.

[4] J. M. Bukowska, M. Jekieek, D. Kruczkowski, T. Ambroy, and J. Jaszczur-Nowicki, "Biomechanical aspects of the foot arch, body balance and body weight composition of boys training football," *Int. J. Environ. Res. Public Health*, vol. 18, no. 9, pp. 5017-5029, May, 2021.

[5] K. Arai, S. l. Ringleb, K. Zhao, L. J. Berglund, H. B. Kitaoka, and K. R. Kaufman, "The effect of flatfootdeformity and tendon loading on the work of friction measured in the posterior tibial tendon," *Clin. Biomech.*, vol. no. 5, pp. 592-600, Jun. 2007.

[6] C. W. Digiovanni, P. Langer, "The role of isolated gastrocnemius and combined achilles contractures in the flatfoot," *Foot Ankle Clini.*, vol. 12, no. 2, pp. 363-379, Jun. 2007.

[7] E. Giza, G. Cush, and L. C. Schon, "The flexible flatfoot in the adult," *Foot Ankle Clini.*, vol. 12, no 2, pp. 251-71, Jun. 2007.

[8] N. A. Smyth, A. A. Aiyer, J. R. Kaplan, C. A. Carmody, and A. R. Kadakia, "Adult-acquired flatfoot deformity," *Eur. J. Orthop. Sur. Traumatol.*, vol. 27, no. 4, pp. 1-7, May, 2017.

[9] C. Neville, A. S. Flemister, J. Houck, "Effects of the Airlift PTTD Brace on Foot kinematics in subjects with stage ii posterior tibial tendon dysfunction," *J. Orthop. Sports Phys. Ther.*, vol. 39, no. 3, pp. 201-209, Apr. 2009.

[10] A. I. Semciw, V. Navamany, C. Ganderton, P. Lawrenson, P. Hodges, J. Kemp, N. J. Collins, "The immediate effect of foot orthoses on gluteal and lower limb muscle activity during overground walking in healthy young adults," *Gait Posture*, vol. 89, no. 52, pp. 102-108, Sep. 2021.

[11] R. Ozmanevra, S. Angin, A. Elvan, and I. Gunal, "Effect of different insole materials on kinetic and kinematic variables of the walking gait in healthy people," *J. Am. Podiatr. Med. Assoc.*, vol. 108, no. 5, pp. 390-396 Jul. 2019.

[12] Y. Zhang, X. Long, J. Du, T. Liu, and X. Lin, "Effect of soft inflatable orthosis on the medial longitudinal arch in patients with flexible flatfoot deformity," *Clini. Biomech.*, vol. 88, no. 1, Aug. 2021.

[13] Tang S, Chen C, Wu C, et al. "The effects of total contact insole with forefoot medial posting on rearfoot movement and foot pressure distributions in patients with flexible flatfoot," *Clini. Neuro. Neurosurg.*, 2015, 129: S8-S11.

[14] J. F. M. Geboers, J. Tuijl, H. A. M. Seelen, M. R. Drost, "Effect of immobilization on ankle dorsiflexion strength," *Scand. J. Rehabil. Med.*, vol. 32, no. 2, pp. 66-71, July, 2000.

[15] J. F. Geboers, M. R. Drost, F. Spaans, H. Kuipers, H. A. Seelen, "Immediate and long-term effects of ankle-foot orthosis on muscle activity during walking: a randomized study of patients with unilateral foot drop," *Arch. Phys. Med. Rehabil.*, vol. 83, no. 2, pp. 240-245, Mar. 2002.

[16] C. D. L. P. Christian, R. Larrainzar-Garijo, and J. Bayod, "Biomechanical stress analysis of the main soft tissues associated with the development of adult acquired flatfoot deformity," *Clini. Biomech.*, vol. 61, pp. 163–171, Dec. 2019.

[17] G. Bao *et al.*, "Corrections to "Academic Review and Perspectives on Robotic Exoskeletons"," in *IEEE Trans. Neural Syst. Rehabil. Eng.*, vol. 28, no. 3, pp. 768-769, March 2020, doi: 10.1109/TNSRE.2020.2974032.

[18] Y. Tu, A. Zhu, J. Song, X. Zhang and G. Cao, "Design and Experimental Evaluation of a Lower-Limb Exoskeleton for Assisting Workers With Motorized Tuning of Squat Heights," in *IEEE Trans. Neural Syst. Rehabil. Eng.*, vol. 30, pp. 184-193, 2022, doi: 10.1109/TNSRE.2022.3143361.

[19] Park Y. L., *et al.*, "Design and control of a bio-inspired soft wearable robotic device for ankle–foot rehabilitation," *Bioinspir. Biomim.*, vol. 9, no. 1, Jan. 2014.

[20] J. Zhang, *et al.*, "Human-in-the-loop optimization of exoskeleton assistance during walking," *Science*, vol. 356, no. 6344, pp. 1280–1284, Jun. 2017.

[21] S. Sridar, *et al.*, "A Soft-Inflatable Exosuit for Knee Rehabilitation: Assisting Swing Phase During Walking," *Front. Robot. AI*, 2018, vol. 5, May, 2018, DOI:10.3389/frobt.2018.00044.

[22] D. Wang *et al.*, "Design and Preliminary Validation of a Lightweight Powered Exoskeleton During Level Walking for Persons With Paraplegia," in *IEEE Trans. on Neural Syst. Rehabil. Eng.*, vol. 29, pp. 2112-2123, 2021, doi: 10.1109/TNSRE.2021.3118725.

[23] M. K. Boes, R. E. Bollaert, R. Kesler, Y. C. Learmonth, M. Islam, M. N. Petrucci. "Six-minute walk performance in persons with multiple sclerosis while using passive or powered ankle-foot orthoses," *Arch. Phys. Med. Rehabil.*, vol. 99, no. 3, Aug. 2017.

[24] S. Hussain, S. Q. Xie and P. K. Jamwal, "Robust Nonlinear Control of an Intrinsically Compliant Robotic Gait Training Orthosis," in *IEEE Trans. Syst. Man Cybern Syst.*, vol. 43, no. 3, pp. 655-665, May 2013.

[25] Y. Zhang, Y. Guo, X. Long, J. Du, X. Lin, "Analysis of the main soft tissue stress associated with flexible flatfoot deformity: a finite element study," *Biomech. Model. Mechanobiol.*, vol. 20, pp. 2169-2177, July, 2021.

[26] E. M. Hoefnagels, M. D. Waites, I. D. Wing, S. M. Belkoff, and B. A. Swierstra, "Biomechanical comparison of the interosseous tibiofibular ligament and the anterior tibiofibular ligament," *Foot Ankle Int.*, vol. 28, no. 5, pp. 602-604, May. 2007.

[27] T. Li, L. Wang, J. Yi, Q. Li and T. Liu, "Reconstructing Walking Dynamics From Two Shank-Mounted Inertial Measurement Units," in IEEE/ASME Transactions on Mechatronics, vol. 26, no. 6, pp. 3040-3050, Dec. 2021.

[28] L. Wang, Y. Sun, Q. Li, T. Liu, J. Yi. "Two Shank-Mounted IMUs-Based Gait Analysis and Classification for Neurological Disease Patients," *IEEE Robot. and Auto. Lett.*, vol. 5, no. 2, pp. 1970-1976, Mar., 2020.

[29] G. S. Murley, H. B. Menz, and K. B. Landorf, "A protocol for classifying normal and flat-arched foot posture for research studies using clinical and radio graphic measurements," *J. Foot Ankle Res.*, vol. 2, no. 1, Feb. 2009, DOI:10.1186/1757-1146-2-22.

[30] J. He , D. Zhang, X. Sheng, S. Li , X Zhu. Invariant Surface EMG Feature Against Varying Contraction Level for Myoelectric Control Based on Muscle Coordination. *IEEE J. Biomed. Health Inform.*, vol. 19, no. 3, 2015, pp. 874-882.

[31] M. Venkadesan, A. Yawar, C. M. Eng, M. A. Dias, D. K. Singh, S. M. Tommasini, "Stiffness of the human foot and evolution of the transverse arch," *Nature*, vol. 579, no. 7797, pp. 97-100, Mar. 2020.

[32] D. A. Nawoczenski, P. M. Ludewig."Electromyographic effects of foot orthotics on selected lower extremity muscles during running," *Arch. Phys. Med. Rehabil.*, 1999, vol. 80, no. 5, pp. 540-544.

[33] G. S. Murley, K. B. Landorf, H. B. Menz. "Do foot orthoses change lower limb muscle activity in flat-arched feet towards a pattern observed in normal-arched feet?" *J. Foot Ankle Res.*, vol. 25, no.7, pp. 728-736.

[34] Y. Guo, Y. Hutabarat, D. Owaki, M. Hayashibe. "Speed variable gait phase estimation during ambulation via temporal convolutional network," *IEEE Sens. J.*, vol. 24, no. 4, pp. 5224-5236.